Controlled Ordering of Topological Charges in an Exciton-Polariton Chain

T. Gao,[1,2] O. A. Egorov,[3,4] E. Estrecho,[1,5] K. Winkler,[3] M. Kamp,[3] C. Schneider,[3] S. Höfling,[3,6] A. G. Truscott,[7] and E. A. Ostrovskaya[1,5]

[1]*Nonlinear Physics Centre, Research School of Physics and Engineering, The Australian National University, Canberra, ACT 2601, Australia*

[2]*Institute of Molecular Plus, Tianjin University, 300072 Tianjin, China*

[3]*Technische Physik, Wilhelm-Conrad-Röntgen-Research Center for Complex Material Systems, Universität Würzburg, Am Hubland, D-97074 Würzburg, Germany*

[4]*Institute of Condensed Matter Theory and Optics, Friedrich-Schiller-Universität Jena, Max-Wien-Platz 1, D-07743 Jena, Germany*

[5]*ARC Centre of Excellence in Future Low-Energy Electronics Technologies, The Australian National University, Canberra, ACT 2601, Australia*

[6]*SUPA, School of Physics and Astronomy, University of St. Andrews, St. Andrews KY16 9SS, United Kingdom*

[7]*Laser Physics Centre, Research School of Physics and Engineering, The Australian National University, Canberra, ACT 2601, Australia*

(Received 7 July 2018; published 27 November 2018)

We demonstrate, experimentally and theoretically, controlled loading of an exciton-polariton vortex chain into a 1D array of trapping potentials. Switching between two types of vortex chains, with topological charges of the same or alternating signs, is achieved by appropriately shaping an off-resonant pump beam that drives the system to the regime of bosonic condensation. In analogy to spin chains, these vortex sequences realize either a "ferromagnetic" or an "antiferromagnetic" order, whereby the role of spin is played by the orbital angular momentum. The ferromagnetic ordering of vortices is associated with the formation of a persistent chiral current. Our results pave the way for the controlled creation of nontrivial distributions of orbital angular momentum and topological order in a periodic exciton-polariton system.

DOI: 10.1103/PhysRevLett.121.225302

Introduction.—Microcavity exciton polaritons attract a great deal of interest as an accessible solid-state platform for fundamental studies of nonequilibrium macroscopic quantum systems [1–4], as well as the development of polariton-based optoelectronics [5]. These quasiparticles arise due to hybridization of electron-hole pairs (excitons) and photons in high-quality microcavities with embedded semiconductor quantum wells. The bosonic nature of exciton polaritons allows for the spontaneous formation of macroscopic coherent states—Bose-Einstein condensates (BECs) [6–9].

The spin degree of freedom [4] and tunable interactions between multiply coupled polariton condensates have recently enabled the realization of driven-dissipative bosonic spin lattices [10,11]. In particular, a crossover from an "antiferromagnetic" state (with staggered spins) to a "ferromagnetic" state (with aligned spins) in such polaritonic lattices has been observed. It was shown that these periodic systems are analogous to the Ising spin model, which has ben very successful in describing a wide range of condensed matter phenomena. Furthermore, the creation of periodic polariton arrays with controllable interactions between the nodes has enabled the demonstration of pseudospin lattices, which can be used as analog simulators of XY Hamiltonians [12].

In principle, the role of spin in the spin lattices and polariton simulators can be played by *orbital angular momentum*, provided that the latter is quantized, well defined on a single lattice cell, and controllable. Being a quantum fluid, a polariton condensate can host a wide variety of quantum vortices [13,14] with an integer *topological charge* defined by the phase winding around the vortex core. Polaritons optically injected by several spatially separated and independent off-resonant pump spots can experience phase locking, producing up to 10^2 vortices and antivortices that extend over tens of microns across the sample and remain locked for a long time [15]. However, the polariton vortex lattices demonstrated in experiments so far are characterized by spontaneously created ordering of topological charges, typically resulting in a zero net orbital angular momentum. Recent theoretical studies predict that the ability to control the ordering of topological charges in a periodic polariton lattice could offer information storage and processing capabilities [16], as well as pave the way for the realization of topologically protected edge currents [17].

In this Letter, we employ an exciton-polariton condensate in a 1D buried mesa array of polariton traps [see Fig. 1(a)] [18–21] to observe the formation of exciton-polariton vortex chains. Due to the nonequilibrium character of condensation, controlled loading of polaritons into distinct energy bands can be realized by shaping the optical excitation beam [18,22,23]. Under the conditions of incoherent optical pumping, far off resonance from the exciton polariton

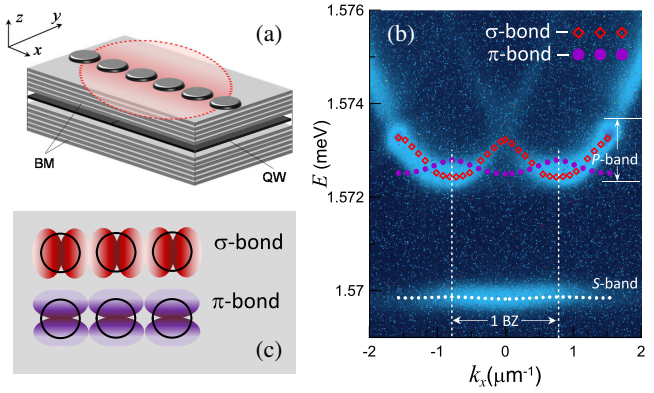

FIG. 1. (a) Schematic of a 1D mesa array microstructured in an AlAs/AlGaAs microcavity formed between two distributed Bragg mirrors (BM) with embedded GaAs quantum wells (QW) illuminated by an off-resonant optical pump (red shaded area, not to scale). (b) Dispersion measurement of the polariton emission from the mesa traps below the condensation threshold. A p energy band consists of two subbands and is formed by the hybridization of the p modes of the individual mesas. Panel (c) shows schematics of the σ-bond and π-bond hybridization forming the p band in panel (b).

energy, we observe vortex chains characterized by different distributions of the topological charge (orbital angular momentum) along the array. By shaping the pump beam, we demonstrate switching between two vortex chains with topological charges of the same or opposite signs. Such topological states represent the vortex analogs of one-dimensional spin systems with ferromagnetic and antiferromagnetic configurations, whereby the role of spin is played by the orbital angular momentum at each lattice site.

Experiment.—The experiment is performed using 1D mesa arrays microstructured in an AlAs/AlGaAs microcavity with 12 GaAs quantum wells, as described in Refs. [18,19,22]. Mesas of $d = 2.0$ μm diameter are separated by a center-to-center distance of $a = 4.0$ μm, with an effective polariton potential depth of ~5.5 meV for each mesa, as sketched schematically in Fig. 1(a). The exciton-polariton condensate is formed spontaneously by pumping the microcavity with a continuous-wave (cw) laser, which injects free carriers well above the exciton energy. The pump beam has a radially symmetric Gaussian intensity profile with a FWHM of 20 μm, and illuminates approximately five mesas in the array. The Rabi splitting in the sample is approximately 13 meV, and the photon-exciton detuning is −13.5 meV (see the Supplemental Material [24]), which means that the exciton polaritons in our experiment have a large photon component.

In the regime of low excitation powers below the condensation threshold, the dispersion (energy vs in-plane momentum) of exciton polaritons reveals the band-gap structure imposed by the periodicity of the trapping potential in the lateral (x) direction, as described in Refs. [18,22]. Both the ground (s) and the excited (p) bands of the characteristic band-gap spectrum of the extended Bloch states can be seen in Fig. 1(b). A large band gap is seen between the ground and the first excited bands, indicating proximity to the tight-binding regime. The most relevant physics arises due to the essentially 2D Bloch states forming via hybridization of the higher-order bound states (p modes) of the individual mesas, marked as p-band in Fig. 1(b). Depending on the spatial orientation of the p modes with respect to the array, they hybridize into two distinct Bloch subbands, namely σ-bonding and π-bonding bands [see Fig. 1(c)].

In the regime of strong excitation, the fast energy relaxation towards lower Bloch states is accompanied by stimulated bosonic scattering into selected states with a maximum gain [18]. In our system, the second Bloch band, formed via bonding of the p modes (dipoles) of individual mesas, becomes strongly populated [Figs. 2(a) and 2(d)]. This is due to inefficient energy relaxation for the highly photonic exciton polaritons at large negative detunings [18]. As a rule, condensation occurs in the vicinity of the high-symmetry

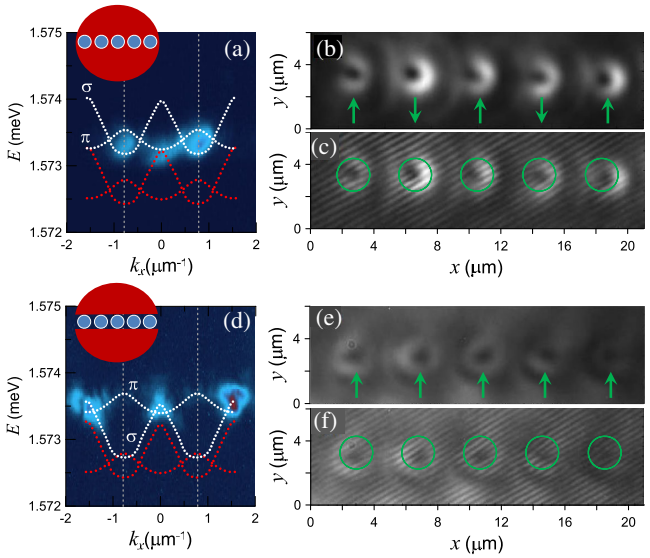

FIG. 2. Photoluminescence above the condensation threshold. (a) Dispersion of exciton polaritons excited by a large-area pump spot (inset, not to scale). Two distinct peaks at the edges of the Brillouin zone (BZ) are visible. The signal in the center of the BZ was detected for $k_y \neq 0$. The dotted white lines represent the calculated dispersion subbands, which are blueshifted with respect to the linear dispersion subbands shown by the red dotted lines. (b) The intensity profile of the antiferromagnetic vortex chain measured in real space and (c) the associated interferometry image. (d) Dispersion of exciton polaritons excited by a large-area pump spot with the mesas shielded by a mask (inset, not to scale). (e) The real-space intensity profile of the ferromagnetic vortex chain and (f) the associated interferometry image. The on-site topological charges +1 and −1 are represented by the up and down arrows, respectively. Lack of circular symmetry in (b) and (e) is due to unequal population of the Bloch modes forming the vortex chain (see text).

points in the dispersion bands corresponding to zero group velocities [25–27], either in the middle of the Brillouin zone (BZ) or at its edges, depending on the particular spatial shape of the pumping spot. As shown below, the spatial distribution of the condensate in the form of the vortex chain can be interpreted as a phase-locked superposition of such 2D, higher-order Bloch states in the array. Therefore, the formation of vortex states in our system is uniquely enabled by the condensation of exciton polaritons into a nonground Bloch state of the 1D array of 2D mesas. Moreover, depending on the pumping conditions, it is possible to populate Bloch states with different symmetries within the same band and, as a consequence, to switch between the vortex chains with "staggered" [Figs. 2(b) and 2(c)] or "aligned" [Figs. 2(e) and 2(f)] topological charges.

In the first configuration, the array of mesa traps is pumped by a large Gaussian pump spot [Fig. 2(a), inset]. At higher pump powers, exciton polaritons undergo a transition to bosonic condensation. The above-threshold dispersion indicates that the σ-bonding band is strongly occupied at the edges of the first BZ ($k_x = \pm\pi/a$) and experiences a blueshift due to the interaction with an incoherent excitonic reservoir injected by the pump [see the dotted white lines in Fig. 2(a)]. An additional subset of occupied states arising from the π-bonding modes is visible in the middle of the BZ ($k_x = 0$) and is detectable only for the $k_y \neq 0$ far-field components of the cavity photoluminescence. Real-space measurements [Figs. 2(b) and 2(c)] show a condensate distribution in the form of a chain of single-charge vortices with alternating signs of the topological charge $(-1, 1, -1, 1, \ldots)$ or, using the spin-chain terminology, an antiferromagnetic configuration. The distribution of the topological charges along the chain is confirmed by using Michelson interferometry, whereby one arm of the interferometer undergoes magnification by a factor of 40 to create a defect-free reference beam [Fig. 2(c)].

In the second configuration, the array of mesa traps is pumped by the same large Gaussian pump spot, but the mesa array itself is shielded from the optical excitation by an optical mask [Fig. 2(d), inset]. The dispersion measurement above the condensation threshold shows that the exciton polaritons occupy the energy states in the middle of the first and the second BZs. In real space and interferometry images, a vortex chain with topological charges $(1, 1, 1, 1, \ldots)$ is observed [Figs. 2(e) and 2(f)], which corresponds to a ferromagnetic configuration. Remarkably, this ferromagnetic ordering signifies the formation of a *chiral state* of the exciton-polariton condensate in the 1D array due to nonzero net orbital angular momentum.

Theory and discussion.—In what follows, we present a simple, intuitive theory of the observed effects. More precisely, we show that a phase-locked superposition of two Bloch states within the highly populated second energy band of the array results in the formation of both the ferromagnetic and antiferromagnetic vortex chains.

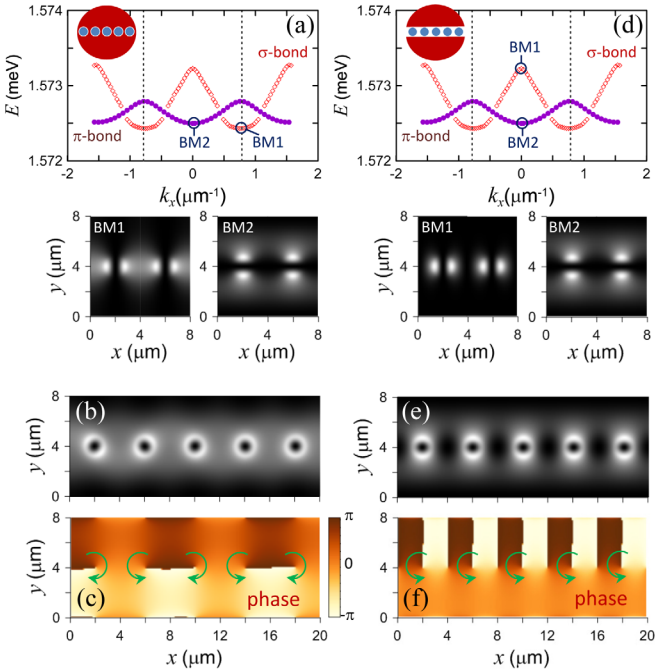

FIG. 3. Calculated Bloch mode dispersions of the p band (a) and (d) and their linear superpositions (b),(c) and (e),(f). (a) σ and π subbands of the chain. Insets in (a) and (d) schematically show the excitation conditions. The circles on the dispersion curves in (a) and (d) mark the Bloch states "BM1" and "BM2" populated by the respective pump spots, with the respective intensity profiles shown on the panels below. (b) Intensity and (c) phase profiles of the linear superposition of the two Bloch modes marked by the circles in panel (a) with the fixed phase difference of $\pi/2$. (e) Intensity and (f) phase profiles of the linear superposition of the two Bloch modes marked by the circles in panel (d) with the fixed phase difference of $\pi/2$.

First, it is instructive to analyze the dispersion relation and the Bloch states of the array in the single-particle linear limit. Solving the standard eigenvalue problem in the photon-exciton basis with the trapping potential for photons [21], we find the dispersion of the Bloch modes within both σ- and π-bonding subbands shown in Figs. 3(a) and 3(d). Without loss of generality, it is convenient to represent the condensate in the polariton basis. Then we can assume that the condensed fraction of the exciton polaritons above threshold can be represented as a superposition of the two Bloch modes:

$$\psi(x, y, t) = a(t)B_\sigma(x, y)e^{-i\omega_a(k_a)t+ik_a x} + b(t)B_\pi(x, y)e^{-i\omega_b(k_b)t+ik_b x}, \quad (1)$$

where the order parameter can be characterized by the complex slowly varying amplitudes $a(t)$ and $b(t)$ associated with the Bloch states $B_\sigma(x, y)$ and $B_\pi(x, y)$ in the σ and π subbands, respectively. Spatial profiles of the selected Bloch modes are shown in Figs. 3(a) and 3(d). The spatial overlap of the Bloch modes with the pump beam determines their effective pumping rates [23].

A large-area pump spot overlaps strongly with both of the subband components, and therefore both components of the condensate are equally occupied. Above the condensation threshold, the exciton polaritons condense into the respective minima of the subbands, namely at the edge of the BZ for the σ subband ($k_a = \pm\pi/a$) and in the middle of BZ for the π subband ($k_b = 0$). Note that the energy difference between these two states in the low-density (linear) limit is vanishingly small, i.e., $\omega_\sigma(\pi/a) - \omega_\pi(0) \approx 0$. As discussed below, the nonlinear effects, such as polariton-polariton and reservoir-polariton interactions, as well as local gain-saturation effects, result in a blueshift and phase locking between these two Bloch modes in the high-density regime. The respective superposition of the Bloch modes with equal amplitudes and a fixed phase of $\pi/2$ forms a sequence of vortices with the alternating charges, as shown in Figs. 3(b) and 3(c). Therefore, similarly to the experiment, a phase-locked state of the two Bloch modes can form an antiferromagnetic chain of vortices.

The situation changes if the array itself is shielded from the optical excitation. In this case, the π subband has a larger overlap with the pump spot due to the spatial orientation of the on-site dipoles. This leads to an imbalance in the effective pumping rates of the two subbands [Fig. 3(d)]. As a result, the polaritons first condense in the π subband in the middle of the BZ ($k_b = 0$) and experience a stronger reservoir-induced blueshift. This blueshift can compensate for the initial linear frequency mismatch between the σ and π Bloch modes, given as $\omega_\pi(0) - \omega_\sigma(0) \neq 0$ [see Fig. 3(d)]. Above the condensation threshold, a superposition of these two Bloch modes with the fixed phase ($\pi/2$) gives rise to the vortex chain with the same topological charges in the ferromagnetic configuration [see Figs. 3(e) and 3(f)].

In order to understand the phase-locking mechanism qualitatively discussed above, it is necessary to consider nonlinear effects. The full dynamics of exciton-polariton condensation in a one-dimensional mesa array for moderate pump powers above threshold can be reliably reproduced by a two-dimensional mean-field dynamical model taking into account energy relaxation due to quantum and thermal fluctuations in the system [28,29]. It consists of the open-dissipative Gross-Pitaevskii equation for the condensate wave function incorporating stochastic fluctuations and coupled to the rate equation for the excitonic reservoir created by the off-resonant cw pump [18,29]. For the sake of simplicity, it is convenient to assume that the incoherent reservoir rapidly reaches a steady state. Under this assumption, the reservoir density can be expressed explicitly as a function of the pump rate and polariton density, and the model becomes closely related to that derived in Ref. [30]. Then, by using the ansatz in the form of Eq. (1), the standard model [28] for the incoherently pumped polaritons with a relevant normalization can be written as follows (see the Supplemental Material [24] for details):

$$
\begin{aligned}
i\frac{da}{dt} &= -\Delta_a a + \Gamma_a a + (\xi_a|a|^2 + 2\xi_{ab}|b|^2)a + \tilde{\xi}_{ab} b^2 a^*, \\
i\frac{db}{dt} &= -\Delta_b b + \Gamma_b b + (\xi_b|b|^2 + 2\xi_{ab}|a|^2)b + \tilde{\xi}_{ba} a^2 b^*,
\end{aligned}
\tag{2}
$$

where $\Gamma_{a,b} = (iR/2 + g_r/\hbar)P_{a,b}/\gamma_r - i\gamma_c/2$, γ_c is the loss rate for the condensed polaritons, g_r accounts for the strength of the blueshift of the coherent polaritons due to their interaction with the incoherent reservoir, γ_r is the loss rate of the incoherent reservoir, R determines the stimulated scattering rate into the condensed state, P_a, P_b are the effective pump rates for the respective Bloch modes, and $\Delta_{a,b} = \omega_{a,b} - \omega_{\sigma,\pi}$. The complex coefficients ξ_a, ξ_b, ξ_{ab}, $\tilde{\xi}_{ab}$, and $\tilde{\xi}_{ba}$ account for both polariton-polariton and reservoir-polariton interactions, as well as the effect of gain saturation due to reservoir depletion.

First, we consider the antiferromagnetic configuration, which is associated with a balanced excitation of both Bloch modes ($P_a = P_b$). Extensive numerical simulations of the model in Eq. (2) with random initial conditions prove the existence of a stable steady-state solution with equal amplitudes $|a| = |b|$ and a fixed phase difference between Bloch modes $\phi_a - \phi_b = \pi/2 + \pi n$, where n is an integer [as shown in Figs. 4(a) and 4(b)]. This confirms the existence of a phase-locked superposition of Bloch modes resulting in the antiferromagnetic vortex chain.

In the case of the ferromagnetic configuration, as discussed above, there is an imbalance in the effective pumping of the two subbands, i.e., $P_a < P_b$. Numerical simulations for the Bloch mode with the nonzero frequency

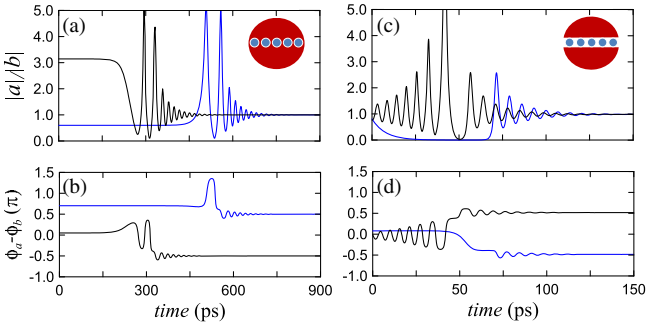

FIG. 4. Nonlinear dynamics of the Bloch mode amplitudes governed by the model in Eq. (2). Panels (a) and (b) show the temporal dynamics of the amplitude ratio and the phase difference between the two Bloch modes, respectively, for the cases of balanced pumping $P_a = P_b = 35$ meV/μm^2 and zero frequency detuning $\Delta_{ab} = \Delta_b - \Delta_a = 0$. Panels (c) and (d) show the temporal dynamics of the amplitude ratio and the phase difference between the two Bloch modes, respectively, for the cases of imbalanced pumping $P_a < P_b$ ($P_a = 32$ meV/μm^2, $P_b = 45$ meV/μm^2) and nonzero frequency detuning $\Delta_{ab} = 0.63$ meV. For other parameters of the model, see the Supplemental Material [24].

detuning at $k_x = 0$ $\Delta_{ab} = \Delta_b - \Delta_b \neq 0$ and imbalanced pumping show that there exist stable states with almost equal amplitudes and locked phase $\phi_a - \phi_b \approx \pi/2 + \pi n$ [as seen in Figs. 4(c) and 4(d)].

Conclusion.—To summarize, we experimentally demonstrate vortex chains with both ferromagnetic and antiferromagnetic distributions of topological charges in an exciton-polariton condensate loaded into a 1D array of mesa traps, and support our observations by a coupled-mode theory for the Bloch states.

This research opens an avenue for using current advanced nanofabrication techniques to create and manipulate stable exciton-polariton vortex chains in microstructured potentials. Furthermore, controlled loading of the exciton-polariton condensate into a topologically ordered state offers interesting possibilities for future realization of topologically protected exciton-polariton currents [17].

The work of the ANU team was supported by the Australian Research Council (ARC) through the Discovery Project No. DP160101371 and the Centre of Excellence CE170100039. The Würzburg group gratefully acknowledges support by the State of Bavaria and funding by the German Research Foundation (DFG Project No. SCHN1376 3.1).

[1] H. Deng, H. Haug, and Y. Yamamoto, Exciton-polariton Bose-Einstein condensation, Rev. Mod. Phys. **82**, 1489 (2010).
[2] I. Carusotto and C. Ciuti, Quantum fluids of light, Rev. Mod. Phys. **85**, 299 (2013).
[3] T. Byrnes, N. Y. Kim, and Y. Yamamoto, Exciton-polariton condensates, Nat. Phys. **10**, 803 (2014).
[4] A. Kavokin, J. J. Baumberg, G. Malpuech, and F. P. Laussy, *Microcavities* (Oxford University Press, New York, 2007).
[5] D. Sanvitto and S. Kéna-Cohen, The road towards polaritonic devices, Nat. Mater. **15**, 1061 (2016).
[6] H. Deng, G. Weihs, C. Santori, J. Bloch, and Y. Yamamoto, Condensation of semiconductor microcavity exciton polaritons, Science **298**, 199 (2002).
[7] J. Kasprzak, M. Richard, S. Kundermann, A. Baas, P. Jeambrun, J. M. J. Keeling, F. M. Marchetti, M. H. Szymańska, R. André, J. L. Staehli, V. Savona, P. B. Littlewood, B. Deveaud, and Le Si Dang, Bose-Einstein condensation of exciton polaritons, Nature (London) **443**, 409 (2006).
[8] R. B. Balili, V. Hartwell, D. Snoke, L. Pfeiffer, and K. West, Bose-Einstein condensation of microcavity polaritons in a trap, Science **316**, 1007 (2007).
[9] Y. Sun, P. Wen, Y. Yoon, G. Liu, M. Steger, L. N. Pfeiffer, K. West, D. W. Snoke, and K. A. Nelson, Bose-Einstein Condensation of Long-Lifetime Polaritons in Thermal Equilibrium, Phys. Rev. Lett. **118**, 016602 (2017).
[10] H. Ohadi, Y. del Valle-Inclan Redondo, A. Dreismann, Y. G. Rubo, F. Pinsker, S. I. Tsintzos, Z. Hatzopoulos, P. G. Savvidis, and J. J. Baumberg, Tunable Magnetic Alignment between Trapped Exciton-Polariton Condensates, Phys. Rev. Lett. **116**, 106403 (2016).
[11] H. Ohadi, A. J. Ramsay, H. Sigurdsson, Y. del Valle-Inclan Redondo, S. I. Tsintzos, Z. Hatzopoulos, T. C. Liew, I. A. Shelykh, Y. G. Rubo, P. G. Savvidis, and J. J. Baumberg, Spin Order and Phase Transitions in Chains of Polariton Condensates, Phys. Rev. Lett. **119**, 067401 (2017).
[12] N. G. Berloff, M. Silva, K. Kalinin, A. Askitopoulos, J. D. Töpfer, P. Cilibrizzi, W. Langbein, and P. G. Lagoudakis, Realizing the classical XY Hamiltonian in polariton simulators, Nat. Mater. **16**, 1120 (2017).
[13] K. G. Lagoudakis, M. Wouters, M. Richard, A. Baas, I. Carusotto, R. Andre, L. S. Dang, and B. Deveaud, Quantized vortices in an exciton-polariton condensate, Nat. Phys. **4**, 706 (2008).
[14] G. Roumpos, M. D. Fraser, A. Löffler, S. Höfling, A. Forchel, and Y. Yamamoto, Single vortex-antivortex pair in an exciton-polariton condensate, Nat. Phys. **7**, 129 (2011).
[15] G. Tosi, G. Christmann, N. G. Berloff, P. Tsotsis, T. Gao, Z. Hatzopoulos, P. G. Savvidis, and J. J. Baumberg, Geometrically locked vortex lattices in semiconductor quantum fluids, Nat. Commun. **3**, 1243 (2012).
[16] X. Ma and S. Schumacher, Vortex-vortex control in exciton-polariton condensates, Phys. Rev. B **95**, 235301 (2017).
[17] H. Sigurdsson, G. Li, and T. C. H. Liew, Spontaneous and superfluid chiral edge states in exciton-polariton condensates, Phys. Rev. B **96**, 115453 (2017).
[18] K. Winkler, O. A. Egorov, I. G. Savenko, X. Ma, E. Estrecho, T. Gao, S. Müller, M. Kamp, T. C. H. Liew, E. A. Ostrovskaya, S. Höfling, and C. Schneider, Collective state transitions of exciton-polaritons loaded into a periodic potential, Phys. Rev. B **93**, 121303(R) (2016).
[19] K. Winkler, J. Fischer, A. Schade, M. Amthor, R. Dall, J. Geßler, M. Emmerling, E. A. Ostrovskaya, M. Kamp, Ch. Schneider, and S. Höfling, A polariton condensate in a photonic crystal potential landscape, New J. Phys. **17**, 023001 (2015).
[20] C. Schneider, K. Winkler, M. D. Fraser, M. Kamp, Y. Yamamoto, E. A. Ostrovskaya, and S. Höfling, Exciton-polariton trapping and potential landscape engineering, Rep. Prog. Phys. **80**, 016503 (2017).
[21] R. I. Kaitouni, O. El Daïf, A. Baas, M. Richard, T. Paraiso, P. Lugan, T. Guillet, F. Morier-Genoud, and J. D. Ganière, J. L. Staehli, V. Savona, and B. Deveaud, Engineering the spatial confinement of exciton polaritons in semiconductors, Phys. Rev. B **74**, 155311 (2006).
[22] T. Gao, E. Estrecho, G. Li, O. A. Egorov, X. Ma, K. Winkler, M. Kamp, C. Schneider, S. Höfling, A. G. Truscott, and E. A. Ostrovskaya, Talbot Effect for Exciton Polaritons, Phys. Rev. Lett. **117**, 097403 (2016).
[23] F. Baboux, L. Ge, T. Jacqmin, M. Biondi, E. Galopin, A. Lemaître, L. Le Gratiet, I. Sagnes, S. Schmidt, H. E. Türeci, A. Amo, and J. Bloch, Bosonic Condensation and Disorder-Induced Localization in a Flat Band, Phys. Rev. Lett. **116**, 066402 (2016).
[24] See Supplemental Material at http://link.aps.org/supplemental/10.1103/PhysRevLett.121.225302 for details on the measurement of photon-exciton detuning low-density dispersion, and theoretical modeling.

[25] C. W. Lai, N. Y. Kim, S. Utsunomiya, G. Roumpos, H. Deng, M. D. Fraser, T. Byrnes, P. Recher, N. Kumada, T. Fujisawa, and Y. Yamamoto, Coherent zero-state and π-state in an exciton-polariton condensate array, Nature (London) **450**, 529 (2007).

[26] D. Tanese, H. Flayac, D. Solnyshkov, A. Amo, A. Lemaître, E. Galopin, R. Braive, P. Senellart, I. Sagenes, G. Malpuech, and J. Bloch, Polariton condensation in solitonic gap states in a one-dimensional periodic potential, Nat. Commun. **4**, 1749 (2013).

[27] E. A. Cerda-Méndez, D. N. Krizhanovskii, M. Wouters, R. Bradley, K. Biermann, K. Guda, R. Hey, P. V. Santos, D. Sarkar, and M. S. Skolnick, Polariton Condensation in Dynamic Acoustic Lattices, Phys. Rev. Lett. **105**, 116402 (2010).

[28] M. Wouters and I. Carusotto, Excitations in a Nonequilibrium Bose-Einstein Condensate of Exciton Polaritons, Phys. Rev. Lett. **99**, 140402 (2007).

[29] M. Wouters, I. Carusotto, and C. Ciuti, Spatial and spectral shape of inhomogeneous nonequilibrium exciton-polariton condensates, Phys. Rev. B **77**, 115340 (2008).

[30] J. M. Keeling and N. G. Berloff, Spontaneous Rotating Vortex Lattices in a Pumped Decaying Condensate, Phys. Rev. Lett. **100**, 250401 (2008).